IOP Publishing Journal of Optics
J. Opt. **16** (2014) 114018 (8pp) doi:10.1088/2040-8978/16/11/114018

Invited Article

Theory of strong coupling between quantum emitters and localized surface plasmons

A Delga, J Feist, J Bravo-Abad and F J Garcia-Vidal[1]

Departamento de Física Teórica de la Materia Condensada and Condensed Matter Physics Center (IFIMAC), Universidad Autónoma de Madrid, E-28049 Madrid, Spain

E-mail: fj.garcia@uam.es

Received 23 June 2014, revised 29 July 2014
Accepted for publication 14 August 2014
Published 3 November 2014

Abstract

We theoretically study the emergence of strong coupling in the interaction between quantum emitters and the localized surface plasmons of a metal nanoparticle. Owing to their quasi-degenerate nature, the continuum of multi-poles is shown to behave as a pseudomode strongly coupled to single emitters instead of as a Markovian bath. We demonstrate that the corresponding capping of the induced loss rate enables collective strong coupling to the dipole mode. Numerical simulations and analytical modeling are applied to several configurations of increasing complexity to grasp the relevant physics. In particular, the emitters closest to the nanoparticle surface are proven to contribute the most to the build-up of the plasmon-exciton polaritons, in contrast with the weak-coupling picture of quenching.

Keywords: nanophotonics, localized surface plasmons, strong coupling, quenching
PACS numbers: 42.50, 73.20, 33.50, 71.35

(Some figures may appear in colour only in the online journal)

1. Introduction

An intriguing property of metal nanoparticles is their ability to confine light inside deep subwavelength volumes in electromagnetic (EM) modes called localized surface plasmons (LSPs). The enhanced light–matter interaction associated with the strong field localization has received a lot of attention in a broad range of contexts, from optical antennas [1], surface-enhanced Raman scattering [2], photovoltaics [3], and biosensing [4] to spasers [5]. In the visible spectrum, light confinement often comes at the price of high metal losses. Investigations of light–matter interactions mediated by LSPs were first restricted to the weak-coupling regime (for example, in fluorescence experiments) [6–8]. However, the quantum properties of surface plasmons have come into focus in the last years [9] and the emergence of strong-coupling regimes characterized by hybrid light–matter states called plasmon-exciton polaritons have been the center of renewed attention. Although the coupling between quantum emitters (QEs) and surface plasmon polaritons supported by a planar surface is relatively well understood [10–14], open questions remain for the case of coupling to LSPs. For instance, theoretical predictions disagree on the relevant LSP involved in strong coupling [15–20], and the debate has not yet been settled by experimental demonstrations because of the complexity of the geometries involved [21–23].

In this paper, we study in-depth the interaction between QEs and the LSP resonances of a spherical metal nanoparticle, focusing on the strong-coupling regime. The system, sketched in figure 1(a), is composed of a spherical metal nanoparticle of radius a surrounded by N QEs (typically atoms, quantum dots, or, in our case, organic molecules). They are modeled as point-dipole two-level systems, with transition energy $\hbar\omega_0$ and dipole moment $\boldsymbol{\mu}$. When excited, they couple to several decay channels: internal nonradiative decay at a rate γ_{QE} (due to rovibrational and phononic effects), spontaneous emission of photons into the modes of the dielectric host material (constant ϵ_d) at a rate $\sqrt{\epsilon_d}\gamma_0$, or

[1] Author to whom any correspondence should be addressed.

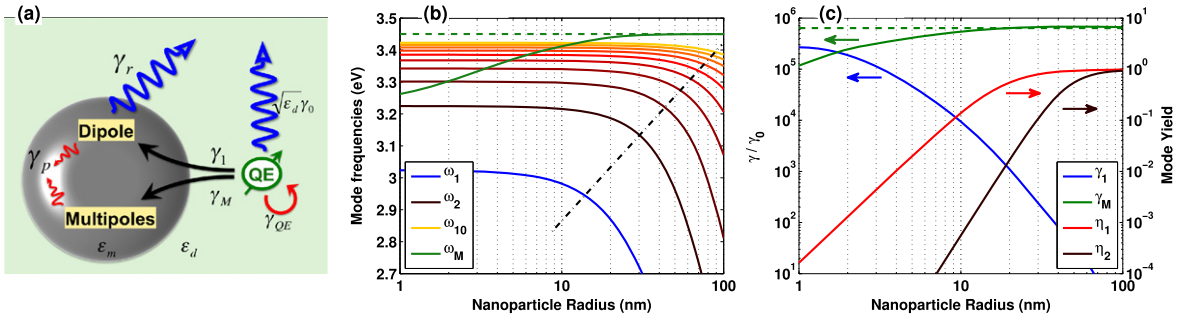

Figure 1. (a): Sketch of the system under study, defining all parameters. (b): Eigenfrequencies of the $l = 1 - 10$ LSP modes as a function of nanoparticle radius a. The green dashed line shows the asymptotic frequency fulfilling the planar condition $\epsilon_m + \epsilon_d = 0$. The black dotted line is a guide for the eye, illustrating the limit of validity for the quasi-static approximation. (c): Left axes, normalized decay rates into the dipole γ_1, and all other multi-poles γ_M for a QE at $h = 1$ nm from the surface of the nanoparticle. The natural frequency of the QE ω_0 is chosen to be resonant with the corresponding mode at ω_1 (dipole frequency) and ω_M (mean frequency of the spectral function for $l \geqslant 2$), as illustrated in matching colors on (b). Right axes, radiative yields of the two lowest LSP modes, calculated as the ratio between scattering and extinction cross sections [25].

excitation of the different LSPs of the nanoparticle whose dielectric constant is characterized by a Drude model $\epsilon_m(\omega) = \epsilon_\infty - \omega_p^2 \Big/ \Big(\omega\Big(\omega + i\gamma_p\Big)\Big)$.

We rely on a Green's function theoretical framework suited to describe lossy systems such as metal nanostructures. This formalism was previously used to investigate the single QE problem [17], then extended to the multiple QE case using multiple-scattering techniques [24]. In both cases, the QE configurations under study were simple to model, yet difficult to attain experimentally. Here, we aim to understand strong-coupling in the more feasible, yet more complex, configuration of a shell of randomly distributed and oriented QEs around the nanoparticle. To do so, we examine several model systems with increasing complexity, revisiting the aforementioned cases along the way. Importantly, at every step, the numerical results are remapped into an effective Hamiltonian to draw analytical insight. After a general presentation of the problem in the weak-coupling picture in section 2, we give an overview of the formalism in section 3. The different configurations are then successively examined, starting with the case of a single QE in section 4. We study two model systems for many QEs in section 5, and finally proceed to the most realistic system in section 6.

2. Weak-coupling regime

In the weak-coupling regime, the total EM decay rate Γ of a QE placed at $\mathbf{r_0}$ is given by $\Gamma = 2\pi J(\mathbf{r_0}, \omega_0)$, where the spectral density is $J(\mathbf{r_0}, \omega) = \omega^2 \Big/ \Big(\pi\hbar\epsilon_0 c^2\Big)\boldsymbol{\mu} \cdot \Im m\mathbf{G}(\mathbf{r_0}, \mathbf{r_0}, \omega) \cdot \boldsymbol{\mu}$ [26]. The dyadic Green's function $\mathbf{G}$ of the classical EM equation

$$\nabla \times \nabla \times \mathbf{G}(\mathbf{r}, \mathbf{r}', \omega) - \frac{\epsilon(\mathbf{r}, \omega)\,\omega^2}{c^2}\mathbf{G}(\mathbf{r}, \mathbf{r}', \omega) = \mathbb{I}\delta(\mathbf{r}, \mathbf{r}') \qquad (1)$$

has two contributions $\mathbf{G} = \mathbf{G_d} + \mathbf{G_{NP}}$, respectively the homogeneous dielectric contribution and the scattered contribution due to the nanoparticle. $\mathbf{G_{NP}}$ can be expanded by angular momentum l using the electrical (TM) Mie spherical harmonics [25][2]. For metal nanoparticles, each angular momentum l supports an LSP resonance. The LSP eigenfrequencies ω_l are displayed in figure 1(b): they are constant for small radii and redshift as the nanoparticle becomes larger. Simultaneously, the radiative losses (rate γ_l^r) increase and overcome the nonradiative (Ohmic) losses (rate γ_l^{nr}), as illustrated by the saturation of the radiative yield $\eta_l = \gamma_l^r/(\gamma_l^r + \gamma_l^{nr})$ shown in figure 1(c). Physically, the frequency redshift (Lamb shift) and increased radiative losses both arise from the enhanced coupling to the vacuum modes for large nanoparticles. Higher-order multi-poles, being more confined at the surface of the nanoparticle, couple less strongly to the vacuum EM modes and have weaker radiative losses: η_l drops by several orders of magnitude for each increment of l, so that we can safely assume that the only radiative (however faintly) mode is the dipole mode, i.e., $\gamma_l^r \approx 0$, for $l \geqslant 2$. Here and in the following, we model a silver nanoparticle with Drude parameters $\epsilon_\infty = 4.6$ eV, and $\hbar\gamma_p = 0.1$ eV, and $\hbar\omega_p = 9$ eV[27], and a host dielectric with $\epsilon_d = 2.13$ [5]. We also choose to use QEs with low quantum yield, having $\mu = 0.38$ e.nm (corresponding to a free-space emission rate $\hbar\gamma_0 = 1\ \mu$eV at $\hbar\omega = 3$ eV), and $\hbar\gamma_{QE} = 15$ meV [28], to demonstrate the robustness of our main conclusions.

The expansion of the spectral density in terms of LSPs enables us to distinguish between the decay rate into the dipole mode γ_1 and into all other multi-pole modes γ_M. These rates are shown in figure 1(c) with varying nanoparticle radius a for a QE placed at $h = r_0 - a = 1$ nm away from the nanoparticle surface. The decay from the QE to the dipole mode becomes faster as the nanoparticle radius shrinks, illustrating the underlying trade-off behind the choice of nanoparticle radius for experimental observation of strong coupling. In the following, we choose a radius $a = 7$nm [5].

[2] The azimuthal momentum m, fully considered in the general approach, can be traced out in the weak-coupling or single QE problems. The contribution of magnetic (TE) resonances will always be negligible for the small nanoparticle considered here.

When placed so close to the nanoparticle, the QEs decay more efficiently into the continuum of multi-poles than into the dipole mode (in figure 1(c), $\gamma_M \gg \gamma_1$ as long as $h < a$). Indeed (not shown), γ_M diverges as h^{-3} whereas γ_1 saturates for $h \to 0$. This fast decay into a continuum of nonradiative modes, characteristic of the so-called quenching regime, can be thought of as an efficient loss channel that makes strong-coupling regimes almost unattainable. In the following, we find that, on the contrary, quenching regions are precisely the most favorable to reach strong-coupling regimes. Actually, the weak-coupling picture breaks down when the coupling process between QEs and LSPs becomes faster than all decoherence processes ($\gamma_1, \gamma_M \approx \gamma_{QE}, \gamma_p, \gamma_1^r$). A strong-coupling treatment is then required.

Before presenting our strong-coupling formalism, we provide further analytical insight into the preceding discussion by means of the quasi-static limit, valid for QEs close to small nanoparticles ($h, a \ll \lambda$), when the coupling of the LSPs to the vacuum EM modes is negligible compared to Ohmic losses [29]. The radial term of the Green's function can then be rewritten as

$$\mathbf{G}^{rr}(r, r, \omega) = \frac{i\sqrt{\epsilon_d}\omega}{6\pi c} + \frac{c^2}{4\pi\omega^2\epsilon_d a^3}\sum_{l=1}^{\infty}\frac{(l+1)^2}{(1+\zeta)^{2l+4}}\frac{\epsilon_m - \epsilon_d}{\epsilon_m + \frac{l+1}{l}\epsilon_d}, \quad (2)$$

where $\zeta = h/a$ is the reduced distance to the nanoparticle surface. In this expression, the divergent real part of $\mathbf{G}_\mathrm{d}(r, r, \omega)$ has been renormalized—in the following, we assume that the induced Lamb shift is already included in the transition energies of the QEs. For a QE with dipole moment oriented parallel to the surface, the $(l+1)^2$ factor is replaced by $l(l+1)/2$. The eigenfrequencies ω_l become only material-dependent, characterized by the well-known condition $\epsilon_m + \frac{l+1}{l}\epsilon_d = 0$. All nanoparticle modes having similar Ohmic losses but different radiative losses, the quasi-static limit is more easily reached for high-order multi-poles as clearly shown by the black dotted line in figure 1(b). Our radius $a = 7$ nm guarantees the validity of the quasi-static limit for all nanoparticle modes, enabling us to derive analytical formulas.

3. Theoretical formalism

In this section, we sketch the main ideas of the formalism, referring the interested reader to the details presented in the supplemental material of ref. [24]. It is based on a macroscopic QED framework [30, 31] suited to describe lossy media. The Hamiltonian of the bare system without QEs is first diagonalized on the basis of the polaritonic operators $\hat{\mathbf{f}}(\mathbf{r}, \omega)$, which represents the elementary excitations of the lossy light–matter system, including all the EM modes of the vacuum and LSPs. All EM information about the metal nanoparticle is remapped into the classical Green's function $\mathbf{G}(\mathbf{r}, \mathbf{r}', \omega)$, as readily seen in the expression of the *E*-field operator

$$\hat{\mathbf{F}}^{(+)}(\mathbf{r}) = i\sqrt{\frac{\hbar}{\pi\epsilon_0}}\int_0^\infty d\omega\frac{\omega^2}{c^2}\int d^3\mathbf{r}'\sqrt{\epsilon^I(\mathbf{r}', \omega)}\,\mathbf{G}(\mathbf{r}, \mathbf{r}', \omega)\hat{\mathbf{f}}(\mathbf{r}', \omega), \quad (3)$$

where $\epsilon^I(\mathbf{r}, \omega)$ is the imaginary part of $\epsilon(\mathbf{r}, \omega)$. Physically, equation (3) can be understood in terms of fluctuational electrodynamics: the *E*-field results from the propagation of the elementary fluctuations occurring in the lossy material. The QEs are then introduced using fermionic operators $\hat{\sigma}_n$ that interact with the *E*-field through dipolar coupling, leading to the full Hamiltonian

$$\mathcal{H} = \int d^3\mathbf{r}\int_0^\infty d\omega\hbar\omega\hat{\mathbf{f}}^\dagger(\mathbf{r}, \omega)\hat{\mathbf{f}}(\mathbf{r}, \omega) + \sum_{n=1}^{N}\frac{\hbar\Omega_n}{2}\hat{\sigma}_n^z - \sum_{n=1}^{N}\left[\hat{\sigma}_n^+ + \hat{\sigma}_n^-\right]\boldsymbol{\mu}_n \cdot \left(\hat{\mathbf{F}}^{(+)}(\mathbf{r}) + \hat{\mathbf{F}}^{(-)}(\mathbf{r})\right), \quad (4)$$

where $\Omega_n = \omega_0 - i\gamma_{QE}/2$. Such a complex eigenenergy is a reasonable treatment for decoherence processes (decay and dephasing) as far as the coherent part of the dynamics is concerned—similarly to the case when a Lindblad master equation is remapped into a non-Hermitian effective Hamiltonian [32]. Note that no rotating-wave approximation is made in the coupling term and that direct dipole–dipole interactions are naturally included through the $\mathbf{G_d}$ component of the Green's function.

Following a procedure introduced for nondispersive, lossless media [33], we perform a Laplace transform on the Heisenberg equations of motion and trace out the fermionic operators $\hat{\sigma}_n$ to obtain a Lippman–Schwinger equation for $\hat{\mathbf{F}}$, where the QEs appear as point scatterers and quantum source operators. In the process, the hypothesis of the low excitation regime is used to approximate the $\hat{\sigma}_n$ as bosonic and the *E*-field operators are obtained using multiple-scattering techniques. Note that in the low excitation regime, it is actually impossible to distinguish between the fermionic and bosonic nature of the QEs, meaning that the physics investigated here with a quantum formalism could also be accounted for by a classical treatment using damped harmonic oscillators.

The emergence of strong coupling is analyzed for the spontaneous emission problem[3] where the physical magnitude of experimental relevance is the light spectrum measured at the detector position, $S(\mathbf{R}, \omega) = \left\langle \hat{\mathbf{F}}^\dagger(\mathbf{R}, \omega) \cdot \hat{\mathbf{F}}(\mathbf{R}, \omega) \right\rangle$. To mimic typical experimental setups where the QEs are incoherently pumped at high energies, we separately calculate the light spectra for the n_0^{th} QE being initially excited, and then sum incoherently over n_0: $S(\mathbf{R}, \omega) = \sum_{n_0}|b_{n_0}|^2 S_{n_0}(\mathbf{R}, \omega)$. The amplitudes b_{n_0} are proportional to $\mu_{n_0} \cdot \mathbf{F}_i(\mathbf{r}_{n_0})$, where $\mathbf{F}_i$ is the (classical) *E*-field amplitude of an incoming plane wave scattered by the nanoparticle. The expression for the light

[3] Scattering problems can also be addressed, see [34].

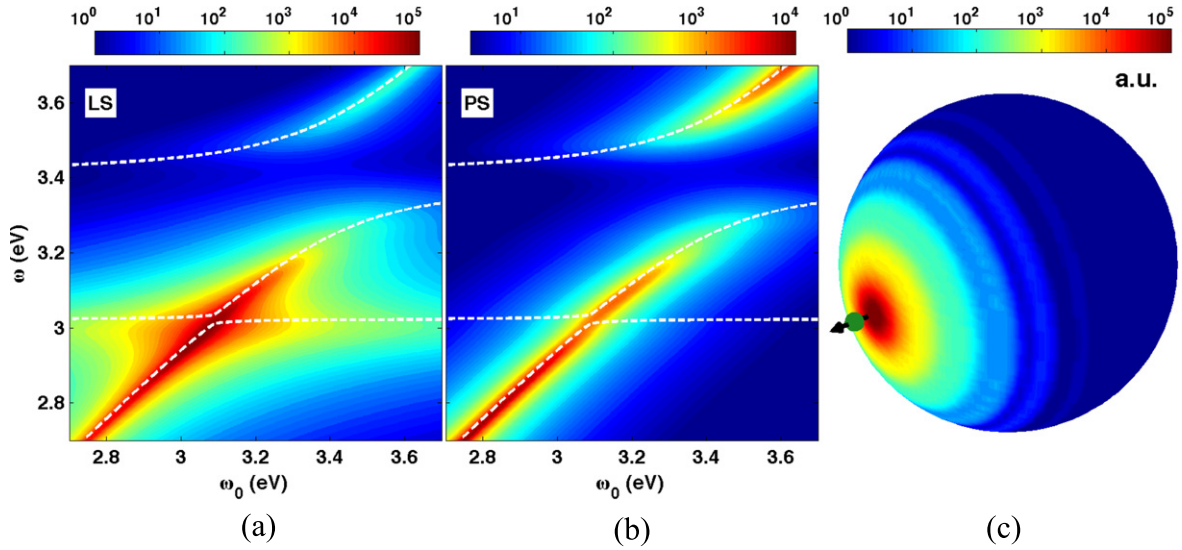

Figure 2. Contour plot of (a) far-field light spectra and (b) near-field polarization spectra as a function of QE frequency for a radial single QE placed 1 nm away from the surface of the nanoparticle. The real parts of the eigenvalues of the Hamiltonian in equation (9) are plotted in white dashed lines. (c): Spatial distribution of the light spectrum on the surface of the nanoparticle for $\omega_0 = \omega = 3.4$ eV.

spectrum with the n_0^{th} QE initially excited is given by

$$S_{n_0}(\mathbf{R}, \omega) = \sum_n \left| \frac{\omega^2}{\epsilon_0 c^2} \mathbf{G}^{(N)}(\mathbf{R}, \mathbf{r}_n, \omega) \boldsymbol{\mu}_n \right|^2 \times \left(\frac{\delta_{n,n_0}}{|\omega - \Omega_n|^2} + \frac{1-\delta_{n,n_0}}{|\omega + \Omega_n|^2} + \frac{\delta_{n,n_0}}{|\omega + \Omega_n|^2} \right), \quad (5)$$

where $\mathbf{G}^{(N)}(\mathbf{R}, \mathbf{r}_n, \omega)$ is the N-scattering dressed Green's function describing the full propagation from the nth QE to the detector. This result is analytical and valid in both weak- and strong-coupling regimes. To deconvolve the effect of propagation to the detector, it is interesting to study the polarization spectra in the m^{th} QE $P^m(\omega) = \left\langle \hat{\sigma}_m^+(-\omega)\hat{\sigma}_m^-(\omega) \right\rangle = \sum_{n_0} |b_{n_0}|^2 P_{n_0}^m(\omega)$, which corresponds to the light spectrum at the QE's position

$$P_{n_0}^m(\omega) = \frac{1}{|\omega - \Omega_m|^2} \Bigg[\delta_{m,n_0} \left(1 - 2\Re e \left\{ \frac{\omega^2}{\hbar \epsilon_0 c^2} \boldsymbol{\mu}_m \mathbf{G}^{(N)}(\mathbf{r}_m, \mathbf{r}_m, \omega) \boldsymbol{\mu}_m \frac{1}{\omega - \Omega_m} \right\} \right) + \sum_n \left| \frac{\omega^2}{\hbar \epsilon_0 c^2} \boldsymbol{\mu}_m \mathbf{G}^{(N)}(\mathbf{r}_m, \mathbf{r}_n, \omega) \boldsymbol{\mu}_n \right|^2 \left(\frac{\delta_{n,n_0}}{|\omega - \Omega_n|^2} + \frac{1-\delta_{n,n_0}}{|\omega + \Omega_n|^2} + \frac{\delta_{n,n_0}}{|\omega + \Omega_n|^2} \right) \Bigg]. \quad (6)$$

4. Single QE problem

The case of a single QE captures the essential physics behind the transition from quenching to strong coupling. Indeed, the decay into the nonradiative multi-poles γ_M only appears Markovian because of the weak-coupling approximation that the decoherence of the bath of LSP modes is much faster than the rate of energy exchange. As shown in [17], when γ_M overcomes all decoherence rates, the multi-poles and the QE start to reversibly exchange energy at a rate given by the Rabi frequency Ω_R. In both the light and polarization spectra shown in figure 2, Ω_R characterizes the width of the avoided crossing between upper and lower plasmon-exciton polariton branches around $\omega_0 = \omega = 3.4$ eV. The dipole mode around $\omega = 3$ eV is much less coupled to the QE (there is almost no signature in the near-field spectrum) but nonetheless dominates the far-field, showing the importance of propagation effects.

Somehow surprisingly, as a continuum of EM modes could be expected to always behave like a Markovian bath similarly to the vacuum EM modes, this emergence of strong coupling arises from the *quasi-degenerate* nature of the LSP modes, all converging towards the cut-off frequency ω_∞ where the condition $\epsilon_m + \epsilon_d = 0$ is fulfilled. Consequently, the multi-poles behave effectively as a single pseudomode whose spatial distribution, illustrated in figure 2(c), looks like a hotspot localized just below the QE. This appears clearly in the quasi-static limit. By further expanding the spectral function,

$$J(\omega) \approx \frac{\sqrt{\epsilon_d}\gamma_0}{2\pi} + \sum_{l=1}^{\infty} \frac{g_l^2}{\pi} \frac{\gamma_p/2}{(\omega - \omega_l)^2 + \left(\gamma_p/2\right)^2}, \quad (7)$$

the LSPs appear as Lorentzian modes characterized by their angular momentum l, eigenfrequency $\omega_l = \omega_p / \sqrt{\epsilon_\infty + \epsilon_d (l+1)/l}$, and Ohmic loss rate γ_p. They are coupled to the QE through the constants

$$g_l^2 = \frac{\mu^2 \omega_p}{4\pi\epsilon_0 \hbar a^3} \left(\frac{\omega_l}{\omega_p} \right)^3 \frac{(l+1)^2}{(1+\zeta)^{2l+4}} \left(1 + \frac{1}{2l} \right). \quad (8)$$

Using the approximation that all multi-poles ($l \geqslant 2$) are degenerate at $\omega_M = \sum_{l=2}^{\infty} \omega_l g_l^2 / \sum_{l=2}^{\infty} g_l^2$, they merge into a

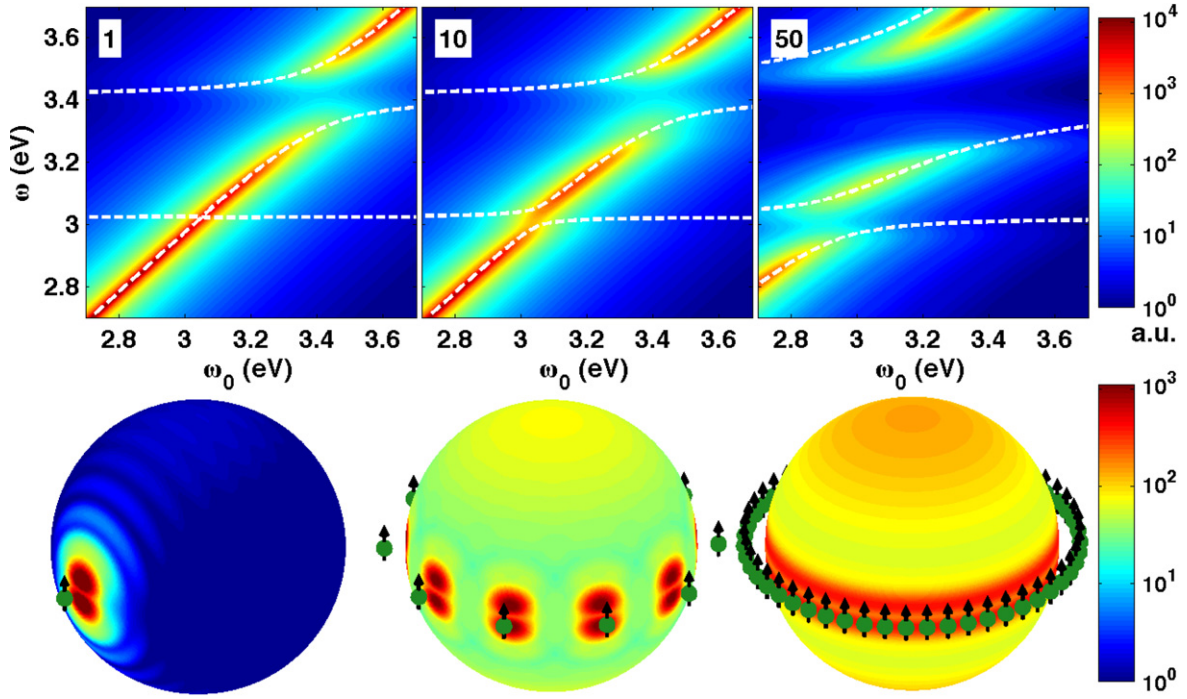

Figure 3. Top: contour plots of the polarization spectra as a function of QE frequency for a equatorial ring of zenithally oriented QEs. Far-field light spectra show similar features. The real parts of the eigenvalues of the Hamiltonian in equation (13) are plotted in white dashed lines. Bottom: corresponding spatial distributions of the light spectrum on the surface of the nanoparticle for $\omega_0 = \omega = 3$ eV.

single Lorentzian, the pseudomode, with coupling constant $g_M = \sqrt{\sum_{l=2}^{\infty} g_l^2}$. The problem can then be remapped into a three-level Hamiltonian $\mathcal{H}_3$ describing the QE, the dipole mode, and the pseudomode

$$\mathcal{H}_3 = \begin{pmatrix} \omega_0 - i\gamma_{QE}/2 & g_1 & g_M \\ g_1 & \omega_1 - i\gamma_p/2 & 0 \\ g_M & 0 & \omega_M - i\gamma_p/2 \end{pmatrix}. \quad (9)$$

This simple analytical model accurately reproduces the results of the full numerics, as seen in figures 2(a)–(b). It highlights the physical cornerstone of the system, i.e., the pseudomode behavior of the multi-poles, which caps the efficiency of quenching at the rate of the Ohmic decay (usually much faster than the QE internal decay).

5. Model systems for a collection of QEs: single layer versus ring configurations

Because of this limited quenching efficiency, a collection of QEs can reach strong-coupling regimes with the more radiative dipole mode. In a previous work, we examined the model system of an homogeneous layer of radial QEs at 1 nm from the surface of the nanoparticle. Here, we recall the main conclusions [24].

As the number of QEs is increased, the strong coupling to the pseudomode disappears from the far-field, while a collective Rabi gap opens at the frequency of the dipole mode. This interplay between collective coupling to dipole and individual coupling to the multi-poles can be grasped by studying the distribution of the relevant nanoparticle modes: localized for the pseudomode, encompassing the entire nanoparticle for the dipole mode. An analytical remapping to a three-level Hamiltonian (collection of QEs, one dipole mode, one pseudomode)

$$\mathcal{H}_3^{Layer} = \begin{pmatrix} \omega_0 - i\gamma_{QE}/2 & g_1\sqrt{N/3} & g_M \\ g_1\sqrt{N/3} & \omega_1 - i\gamma_p/2 & 0 \\ g_M & 0 & \omega_M - i\gamma_p/2 \end{pmatrix}, \quad (10)$$

shows that in the strong-coupling regime, for QEs close to resonance with the dipole mode, the multi-poles act more like an effective detuning δ_{eff} than as a decay channel. Indeed, the Rabi splitting Ω_R between the plasmon-exciton polariton modes is well approximated at resonance ($\omega_0 = \omega_1$) by

$$\Omega_R \approx \sqrt{g_1^2 \frac{N}{3} - \frac{1}{4}\left(\frac{\gamma_{QE} - \gamma_p}{2} + i\delta_{eff}\right)^2}, \quad (11)$$

$$\delta_{eff} = \frac{2g_M^2 \delta_M}{\delta_M^2 + \left(\frac{\gamma_{QE} - \gamma_p}{2}\right)^2}, \quad (12)$$

with $\delta_M = \omega_M - \omega_1$. The threefold degeneracy of the dipole mode explains the factor 3 in its coupling term to the QEs. Additionally, direct dipole–dipole interactions are found to be negligible when the QEs are separated by more than 1 nm.

Having revisited the two previously investigated cases, we now go a step beyond their conclusions and show that other effects can emerge when the QEs are very close to

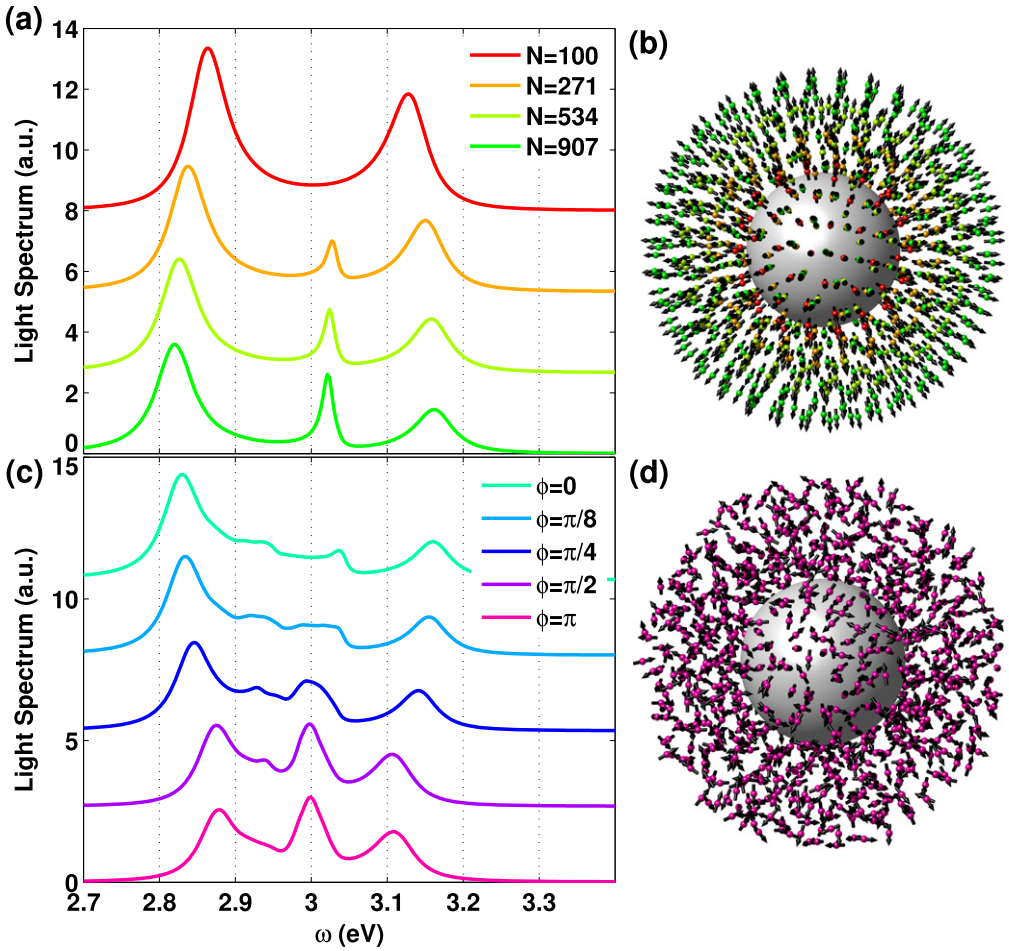

Figure 4. Light spectra (a,c) and spatial configurations (b,d) for a regular stacking of homogeneous layers of radial QEs (a,c) and randomly positioned QEs with increasing noise in their dipole moment orientation (c,d). The light spectra are normalized to a constant incoming illumination. See the main text for details.

one another. To do so, we examine one last model configuration: a ring of QEs at a distance of 1 nm from the equator of the nanoparticle and oriented parallel to the polar axis z (figure 3). As can be seen in the polarization spectrum for 10 QEs, a Rabi gap opens at the dipole frequency around 3 eV, whereas the coupling to the pseudomode remains unchanged. This interplay between collective coupling to the dipole mode and individual coupling to the pseudomode is confirmed by the spatial distribution of the light spectrum, where the E-field distribution of the dipole mode parallel to z emerges from the background below the hotspots corresponding to the nonoverlapping pseudomodes.

However, contrary to the case of the layer, for 50 QEs, the Rabi splitting at the pseudomode frequency increases drastically. In the field map, the corresponding hotspots now overlap, triggering also collective coupling to the pseudomodes. The entire spectrum is additionally blueshifted by direct dipole–dipole interactions [35]. Note that here for sake of simplicity (it is the relevant eigenstate of all parts of the Hamiltonian), instead of the incoherent pumping scheme, we have used a specific starting state where all QEs are in phase and share the same amount of excitation: $|+\rangle = \frac{1}{\sqrt{N}}\sum_n |e_n, 0\rangle$.

Again, these effects can be understood in terms of a three-level Hamiltonian:

$$\mathcal{H}_3^{Ring} = \begin{pmatrix} \omega_0 - i\gamma_{QE}/2 + \delta_0 & g_1\sqrt{N} & g_M + 2g_{\text{eff}} \\ g_1\sqrt{N} & \omega_1 - i\gamma_p/2 & 0 \\ g_M + 2g_{\text{eff}} & 0 & \omega_M - i\gamma_p/2 \end{pmatrix}, \quad (13)$$

where g_1 and g_M are adapted for QEs oriented parallel to the nanoparticle surface. The collective factor is now $\sqrt{N}$ because all QEs couple only to the dipole mode parallel to z. The effective detuning δ_0, induced by Coulombic dipole–dipole interactions, is calculated from the highest eigenvalue of the Hamiltonian, where QEs are coupled through $V_{ij} = (4\pi\epsilon)^{-1}\left(\boldsymbol{\mu}_i \cdot \boldsymbol{\mu}_j / r_{ij}^3 - 3(\boldsymbol{\mu}_i \cdot \mathbf{r}_{\text{ij}})(\boldsymbol{\mu}_j \cdot \mathbf{r}_{\text{ij}}) / r_{ij}^5\right)$. The collective effects for the pseudomodes can be crudely modeled using a tight-binding approach where each QE is also coupled to its two nearest neighbors' pseudomodes through $g_{\text{eff}} = g_M e^{-d^2/(2d_0^2)}$, where d is the distance separating consecutive hotspots centers on the nanoparticle surface and d_0 is the characteristic extension along the equator of the isolated hotspots (extracted using a Gaussian fit). This analytical model qualitatively captures the physics of the full numerics

illustrated in figure 3. The overestimation of the Rabi splitting at the multi-poles frequency most likely comes from the underlying overestimation of the number of independent pseudomodes involved (one for each QE).

6. Toward realistic configurations

In this last section, we incrementally increase the complexity of the system to reach experimentally feasible configurations. Starting from a homogeneous layer of 100 radial QEs at 1 nm from the surface of the nanoparticle (figure 4(b), $N = 100$), we add outer layers ($N = 271$ to $N = 907$) of radial QEs while keeping the volume density of QEs constant. Even if the Rabi splitting in the light spectrum (figure 4(a)) increases slightly, most of the contributions to the strong coupling to the dipole are carried by the innermost QEs. An additional peak corresponding to uncoupled QEs appears, slightly above the QEs' natural frequency ($\omega_0 = 3$ eV), because of direct dipole–dipole interactions.

Keeping the radial orientation, we now randomly distribute the same number of QEs ($N = 907$) in the same shell. In this configuration, labeled $\phi = 0$ in figure 4(c), the two outer peaks corresponding to the strong coupling to the dipole mode remain unchanged, but the central zone now displays a richer phenomenology. We then gradually increase the noise in the QEs' orientation, defining ϕ as the maximum allowed noise angle with the radial direction. Here, $\phi = \pi$ corresponds to the experimentally most easily achievable configuration of randomly distributed and oriented QEs (figure 4(d)). With increasing noise, the Rabi splitting to the dipole mode decreases, whereas the direct emission from the uncoupled QEs grows at $\omega = 3$ eV. Nevertheless, the final configuration still displays a Rabi splitting of around 200 meV, which is well separated from the central peak due to uncoupled QEs. We stress that the innermost QEs are the main contributors to this splitting, even if they only account for 20% of the total QEs.

7. Conclusion

Through the careful analysis of different configurations with varying complexity, we have identified the main effects governing the strong-coupling interaction between QEs and a metal nanoparticle. A single QE can be strongly coupled to a pseudomode consisting of multi-poles LSPs. Their quasi-degenerate nature indeed limits the quenching efficiency to the metal Ohmic loss rate, allowing for the build-up of a collective strong coupling between an assembly of QEs and the more radiative dipole mode that then dominates the far-field. Note that the QEs closest to the nanoparticle, i.e., the supposedly most quenched ones, contribute most to the Rabi splitting detectable in the far-field. Some second-order collective effects are also involved in the coupling to the multi-poles when the emitters are very densely packed, and direct dipole–dipole interactions account for an overall blueshift of the relevant bright states.

Our results show that to reach strong-coupling regimes between QEs and LSPs, the relevant LSP is the dipole mode, because it can benefit from collective coupling from all QEs and is by far the most radiative nanoparticle mode. The critical quantity governing the choice of QE is thereby the density of dipole moment μ, whereas QE internal decay or dephasing rate γ_{QE} are less relevant because they are usually negligible compared to the more demanding Ohmic loss rate γ_{p}.

Acknowledgments

This work has been funded by the European Research Council (ERC-2011-AdG Proposal No. 290981).

References

[1] Bharadwaj P, Deutsch B and Novotny L 2009 Optical antennas *Adv. Opt. Photon.* **1** 438–83
[2] Kneipp K, Kneipp H, Itzkan I, Dasari R R and Feld M S 2002 Surface-enhanced raman scattering and biophysics *J. Phys.: Condens. Matter.* **14** R597
[3] Atwater H A and Polman A 2010 Plasmonics for improved photovoltaic devices *Nature Mater.* **9** 205–13
[4] Anker J N, Hall W P, Lyandres O, Shah N C, Zhao J and van Duyne R P 2008 Biosensing with plasmonic nanosensors *Nature Mater.* **7** 442–53
[5] Noginov M A, Zhu G, Belgrave A M, Bakker R, Shalaev V M, Narimanov E E, Stout S, Herz E, Suteewong T and Wiesner U 2009 Demonstration of a spaser-based nanolaser *Nature* **460** 1110–2
[6] Dulkeith E, Morteani A C, Niedereichholz T, Klar T A, Feldmann J, Levi S A, van Veggel F C J M, Reinhoudt D N, Möller M and Gittins D I 2002 Fluorescence quenching of dye molecules near gold nanoparticles: radiative and nonradiative effects *Phys. Rev. Lett.* **89** 203002
[7] Anger P, Bharadwaj P and Novotny L 2006 Enhancement and quenching of single-molecule fluorescence *Phys. Rev. Lett.* **96** 113002
[8] Kühn S, Håkanson U, Rogobete L and Sandoghdar V 2006 Enhancement of single-molecule fluorescence using a gold nanoparticle as an optical nanoantenna *Phys. Rev. Lett.* **97** 017402
[9] Tame M S, McEnery K R, Özdemir Ş K, Lee J, Maier S A and Kim M S 2013 Quantum plasmonics *Nature Physics* **9** 329–40
[10] Bellessa J, Bonnand C, Plenet J C and Mugnier J 2004 Strong coupling between surface plasmons and excitons in an Organic semiconductor *Phys. Rev. Lett.* **93** 036404
[11] Vasa P *et al* 2008 Coherent exciton-surface-plasmon-polariton interaction in hybrid metal-semiconductor nanostructures *Phys. Rev. Lett.* **101** 116801
[12] Schwartz T, Hutchison J A, Genet C and Ebbesen T W 2011 Reversible switching of ultrastrong light-molecule coupling *Phys. Rev. Lett.* **106** 196405
[13] González-Tudela A, Huidobro P A, Martín-Moreno L, Tejedor C and García-Vidal F J 2013 Theory of strong coupling between quantum emitters and propagating surface plasmons *Phys. Rev. Lett.* **110** 126801
[14] González-Tudela A, Huidobro P A, Martín-Moreno L, Tejedor C and García-Vidal F J 2014 Reversible dynamics of single quantum emitters near metal-dielectric interfaces *Phys. Rev.* B **89** 041402(R)

[15] Trügler A and Hohenester U 2008 Strong coupling between a metallic nanoparticle and a single molecule *Phys. Rev.* B **77** 115403
[16] Waks E and Sridharan D 2010 Cavity qed treatment of interactions between a metal nanoparticle and a dipole emitter *Phys. Rev.* A **82** 043845
[17] van Vlack C, Kristensen P T and Hughes S 2012 Spontaneous emission spectra and quantum light-matter interactions from a strongly coupled quantum dot metal-nanoparticle system *Phys. Rev.* B **85** 075303
[18] Dvoynenko M M and Wang J K 2013 Revisiting strong coupling between a single molecule and surface plasmons *Opt. Lett.* **38** 760–2
[19] Nerkararyan K V and Bozhevolnyi S I 2014 Relaxation dynamics of a quantum emitter resonantly coupled to a metal nanoparticle *Opt. Lett.* **39** 1617–20
[20] Savasta S, Saija R, Ridolfo A, di Stefano O, Denti P and Borghese F 2010 Nanopolaritons: vacuum rabi splitting with a single quantum dot in the center of a dimer nanoantenna *ACS Nano* **4** 6369–76
[21] Sugawara Y *et al* 2006 Strong coupling between localized plasmons and organic excitons in metal nanovoids *Phys. Rev. Lett.* **97** 266808
[22] Fofang N T, Park T H, Neumann O, Mirin N A, Nordlander P and Halas N J 2008 Plexcitonic nanoparticles: plasmon & exciton coupling in nanoshell & j-aggregate complexes *Nano Letters* **8** 3481–7
[23] Schlather A E, Large N, Urban A S, Nordlander P and Halas N J 2013 Near-field mediated plexcitonic coupling and giant rabi splitting in individual metallic dimers *Nano Letters* **13** 3281–6
[24] Delga A, Feist J, Bravo-Abad J and Garcia-Vidal F J 2014 Quantum emitters near a metal nanoparticle: strong coupling and quenching *Phys. Rev. Lett.* **112** 253601
[25] Bohren C F and Huffman D R 2008 *Absorption and Scattering of Light by Small Particles* (John Wiley & Sons)
[26] Novotny L and Hecht B 2012 *Principles of Nano-optics* (Cambridge University Press)
[27] Palik E D 1998 *Handbook of Optical Constants of Solids* vol 3 (Academic Press)
[28] Fidder H, Knoester J and Wiersma D A 1990 Superradiant emission and optical dephasing in j-aggregates *Chem. Phys. Lett.* **171** 529–36
[29] Francs G C d, Bouhelier A, Finot E, Weeber J C, Dereux A, Girard C and Dujardin E 2008 Fluorescence relaxation in the near-field of a mesoscopic metallic particle: distance dependence and role of plasmon modes *Optics Express* **16** 17654–66
[30] Huttner B and Barnett S M 1992 Quantization of the electromagnetic field in dielectrics *Phys. Rev.* A **46** 4306
[31] Dung H T, Knöll L and Welsch D G 1998 Three-dimensional quantization of the electromagnetic field in dispersive and absorbing inhomogeneous dielectrics *Phys. Rev.* A **57** 3931
[32] Petruccione F and Breuer H-P 2002 *The Theory of Open Quantum Systems* (Oxford: Oxford University Press)
[33] Wubs M, Suttorp L G and Lagendijk A 2004 Multiple-scattering approach to interatomic interactions and superradiance in inhomogeneous dielectrics *Phys. Rev.* A **70** 053823
[34] Chen X W, Sandoghdar V and Agio M 2013 Coherent interaction of light with a metallic structure coupled to a single quantum emitter: from superabsorption to cloaking *Phys. Rev. Lett.* **110** 153605
[35] Pustovit V N and Shahbazyan T V 2010 Plasmon-mediated superradiance near metal nanostructures *Phys. Rev.* B **82** 075429